Utilization of a Spent FCC Catalyst in Kaolin-Based Ceramics: Sintering Behavior and Phase Evolution

UDC:666.3-187
Original scientific paper https://doi.org/10.46793/aeletters.2026.11.2.4

Ganka Kolchakova[1*], Yancho Hristov[1]

[1]Department of Materials Science, Burgas State University "Prof. Dr. Assen Zlatarov", Bulgaria

Abstract:
Spent fluid catalytic cracking (FCC) catalysts represent an environmental challenge. Due to their high Al_2O_3 and SiO_2 content, they have significant potential for reuse as raw materials and additives in ceramics. In this work, the sintering behaviour, phase evolution and densification of kaolin-based ceramics were studied. Compositions containing 30, 50, and 70 mass% spent FCC catalyst (designated as C_{30}, C_{50}, and C_{70}) were developed. The pressed blends were fired at temperatures between 1250 and 1500°C. X-ray diffraction results show that the C_{50} samples present the highest mullite content, while cristobalite dominates in the C_{70} composition. C_{30} composition achieved the best densification. At 1500°C, they reach an apparent density of 2.38 g/cm^3, an apparent porosity of up to 5.4% and water absorption of 2.3%. The decrease in surface area of the C_{30} sample—from 58.9 m²/g in the raw state to 1.3 m²/g after firing at 1250°C—confirms effective sintering. These results show that the spent FCC catalyst is an effective additive in ceramic production.

ARTICLE HISTORY
Received: 16 April 2026
Revised: 19 June 2026
Accepted: 25 June 2026
Published: 29 June 2026

KEYWORDS
Spent FCC catalyst, Kaolin, Ceramics, Sintering, Phase evolution, Mullite

1. INTRODUCTION

Large oil and gas processing plants are essential to the global energy infrastructure, relying on specialized catalysts and sorbents to ensure efficient and selective chemical transformations [1]. Alumina-based catalysts are indispensable for hydrotreating processes [2], while zeolites, especially type Y, are fundamental to FCC—a crucial process for converting heavy petroleum fractions into valuable gasoline and light olefins [3-5]. After their service life, these catalysts become deactivated and are classified as spent catalysts, often ending up in landfills. This disposal practice poses a significant and growing environmental challenge due to the potential leaching of heavy metals (e.g., Ni, V, and Mo) into soil and groundwater, alongside the occupation of land space [6]. Economically, this represents a loss of valuable materials and incurs high disposal costs [7]. With the annual global volume of spent refinery catalysts estimated at hundreds of thousands of tons, developing sustainable valorization strategies within a circular economy framework is critical [8].

A promising route for the utilization of these materials is their incorporation into ceramic and refractory products [9]. The ceramic industry possesses significant capacity and technological adaptability to utilize suitable secondary materials [10-12]. Many industrial wastes have a composition similar to traditional clays and feldspars, allowing them to act as functional additives without compromising the final product's properties [13].

Waste zeolite catalysts represent a particularly valuable resource due to their high silica (SiO_2) and alumina (Al_2O_3) content [14]. Their application as aluminosilicate additives in ceramic matrices can significantly enhance the microstructure and high-temperature technical properties, such as thermal stability and mechanical strength. Incorporating these wastes into higher-end ceramics, particularly refractories, mitigates environmental impacts and reduces the consumption of virgin raw materials,

*CONTACT: Ganka Kolchakova, e-mail: ganka-kolchakova@uniburgas.bg

presenting a highly effective strategy for waste valorization [15].

Despite the recognized potential of spent FCC catalysts as secondary raw materials, their specific high-temperature sintering behavior when introduced into kaolin matrix remains insufficiently investigated. While previous research has predominantly focused on low-temperature applications such as traditional building ceramics, the high Al_2O_3 and SiO_2 content of these catalysts makes them highly suitable for refractory applications, where the formation of phases like mullite and cristobalite determines thermal and mechanical performance. Therefore, the present study aims to investigate and evaluate the thermal transformations, phase evolution, and densification of kaolin-based ceramics incorporating varying amounts (30, 50, and 70 mass%) of a spent FCC catalyst. By firing the mixtures at high temperatures (1250–1500 °C), this work assesses the role of the catalyst in the sintering process and determines the optimal composition for producing dense, stable ceramic materials.

2. MATERIALS AND METHODS

2.1. Materials and Sample Preparation

The raw materials used in this study were a spent zeolite-based FCC catalyst powder, supplied by BASF, and a commercially available kaolin (grade "BO extra", from the "Kaolin" deposit, Senovo, Bulgaria). The spent catalyst originated from gasoline production and was used as received without additional processing. The chemical compositions of both starting materials were determined by X-ray fluorescence (XRF) analysis and are presented in Table 1. From these raw materials, three mixtures—designated as C_{30}, C_{50}, and C_{70}—were prepared by incorporating 30, 50, and 70 mass% of the spent catalyst into the kaolin, respectively. The calculated chemical compositions of these final mixtures are also given in Table 1. The prepared mixtures were first dry-mixed to ensure homogeneity. For shaping via the semi-dry pressing method, the powders were moistened with distilled water to a moisture content of 8 mass%, homogenized, and uniaxial pressed into cylindrical pellets (22 mm in diameter and a thickness of approximately 8 mm) at 50 MPa using a hydraulic press. The resulting green samples were dried at 110 °C for 24 h to remove residual moisture. Sintering was subsequently carried out in a laboratory chamber furnace (Nabertherm, Germany) at temperatures of 1250, 1350, 1450, and 1500 °C.

Table 1. Chemical composition of the raw materials and calculated composition of the mixtures (mass %)

Materials	Catalyst	Kaolin	C_{30}	C_{50}	C_{70}
Al_2O_3	37.24	34.20	35.11	35.72	36.33
SiO_2	57.46	51.00	52.94	54.23	55.52
K_2O	-	1.20	0.84	0.60	0.36
CaO	-	0.15	0.10	0.07	0.04
Na_2O	0.31	0.15	0.19	0.22	0.26
MgO	-	0.25	0.18	0.13	0.08
Fe_2O_3	0.58	0.80	0.73	0.69	0.64
La_2O_3	1.69	-	0.51	0.85	1.18
REOs	1.74	-	0.52	0.87	1.22
LOI	10.00	12.00	8.40	6.00	3.60

*REOs - Rare Earth Oxides

The firing regime consisted of a constant heating rate of 5 °C/min and a 1-hour isothermal hold at the maximum temperature, followed by natural cooling inside the furnace.

2.2. Characterization Methods

The chemical composition of the spent catalyst and the kaolin was determined by XRF spectrometry at an accredited laboratory Eurotest Control EAD, Sofia, Bulgaria. Nitrogen adsorption isotherms were recorded at 77 K using a Surfer surface area and porosity analyzer (Thermo Scientific). The specific surface area was calculated by the Brunauer–Emmett–Teller (BET) method. The micropore volume was determined by the Dubinin method. The total pore volume and mesopore volume were also calculated from the adsorption data. Simultaneous differential thermal analysis (DTA) and thermogravimetry (TG) were performed on the raw spent catalyst in air up to 1250 °C with a heating rate of 10 °C/min. For the C_{30}–C_{70} samples, differential scanning calorimetry (DSC) was used under the same conditions. X-ray diffraction (XRD) patterns were recorded on a D2 Phaser powder diffractometer using CuKα radiation with a nickel filter in the 2ϑ range of 20–70°. The measurements were performed on the fired samples after firing at 1350 °C. Phase identification was carried out using the Powder Diffraction File (PDF) database (ICDD). Water absorption, apparent density and apparent porosity were determined by the Archimedes method (hydrostatic weighing) according to ISO 5017:2025 [16]. Samples were dried at 110 °C to constant mass, then boiled in distilled water for 2 h to saturate the open pores. The dry mass (m_0),

saturated mass in air (m_1), and mass of the saturated sample suspended in water (m_2) were measured using an analytical balance (±0.0001 g). The following parameters were calculated:

- Water absorption (*WA*)

$$WA = \frac{m_1 - m_0}{m_0}.100, \ (\%) \quad (1)$$

- Apparent density ($\rho_{app.}$)

$$\rho_{app.} = \frac{m_0 \cdot \rho_w}{m_1 - m_2}, \ (\frac{g}{cm^3}) \quad (2)$$

- Apparent porosity ($P_{app.}$)

$$P_{app.} = \frac{m_1 - m_0}{m_1 - m_2}.100, \ (\%) \quad (3)$$

where ρ_w is the density of distilled water at the measurement temperature. For each composition and firing temperature were determined as the average of five tested samples.

The flexural strength was determined according to the standard methodology ISO 5014:2025 [17]. The testing was performed at the standardized laboratory GEOLAB – Sofia.

3. RESULTS AND DISCUSSION

3.1 Characterization of Spent Zeolite-Based Catalyst

The chemical composition of the waste catalyst (Table 1) shows a high content of SiO_2 (57.46 %) and Al_2O_3 (37.24 %), together accounting for nearly 95 % of the total mass. Consistent with previous reports, such an aluminosilicate composition enables the formation of refractory crystalline phases, such as mullite ($3Al_2O_3 \cdot 2SiO_2$), during high-temperature sintering [18, 19].

Nitrogen adsorption–desorption analysis (Fig. 1) displays a Type IV isotherm according to the IUPAC classification, which is characteristic of microporous materials (with the micropore volume accounting for 72.8% of the total pore volume). Furthermore, the presence of an H4-type hysteresis loop confirms the mesopores, a finding confirmed by the pore structure data (Table 2). The specific surface area determined by the BET method is 87 m²/g.

This well-defined micro- and mesoporous network provides significant adsorption capacity and contributes to a higher solid-state reactivity of the material during the initial stages of sintering.

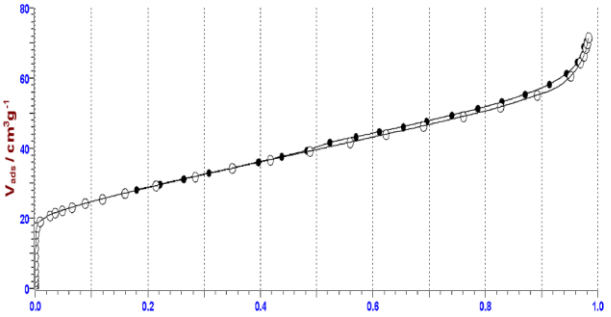

Fig. 1. Nitrogen adsorption isotherm of spent zeolite-based catalyst

Table 2. Textural porous parameters of spent zeolite-based catalyst

S_{BET}, m²/g	$V_{0.95}$, cm³/g	V_{micro}, cm³/g	V_{meso} cm³/g	V_{micro} (%)	V_{meso} (%)
87	0.0489	0.0356	0.0133	72.8	27.2

To establish the changes that occur during the heat treatment of the spent zeolite catalyst, DTA was performed, as presented in Fig. 2. An endothermic effect up to approximately 140 °C is observed, associated with the removal of adsorbed moisture (physically and capillarily-bound water) from the material.

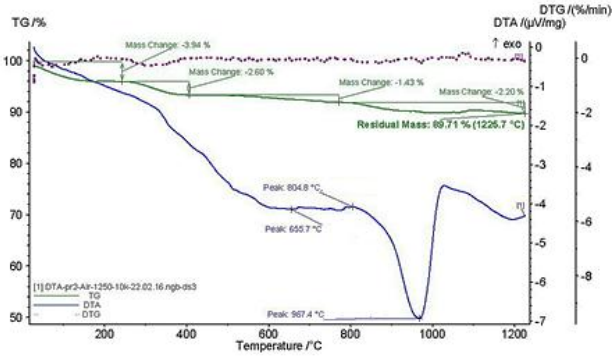

Fig. 2. Thermal behavior of the spent zeolite-based catalyst

In the temperature range 250-900 °C, the TG curve shows a gradual mass loss totalling about 10%, likely due to the combustion of carbon compounds [20]. At a temperature of 967 °C, a distinct endothermic peak is observed, associated with the destruction of the crystalline structure of the zeolite and the formation of an amorphous phase [7]. This is followed by a broad exothermic peak at around 1100 °C, which is characteristic of crystallization transformations and most likely the formation of mullite ($Al_2O_3 \cdot SiO_2$) [18].

The X-ray diffraction pattern of the spent catalyst (Fig. 3) exhibits distinct reflections characteristic of a zeolitic structure with a partially preserved crystalline framework. The identified

peaks correspond to a phase with an approximate composition $Al_{4.73}Si_{43.3}O_{96}$, indicating a high-silica character of the material (Si/Al ≈ 9.2). Such a composition is typical for dealuminated zeolitic systems, where thermal or hydrothermal treatment during the catalytic process leads to the extraction of aluminum atoms from the tetrahedral positions of the framework [20]. As a result of this dealumination process, a partial amorphization of the zeolitic structure occurs, leading to the formation of a silico–aluminous matrix containing residual crystalline domains [20].

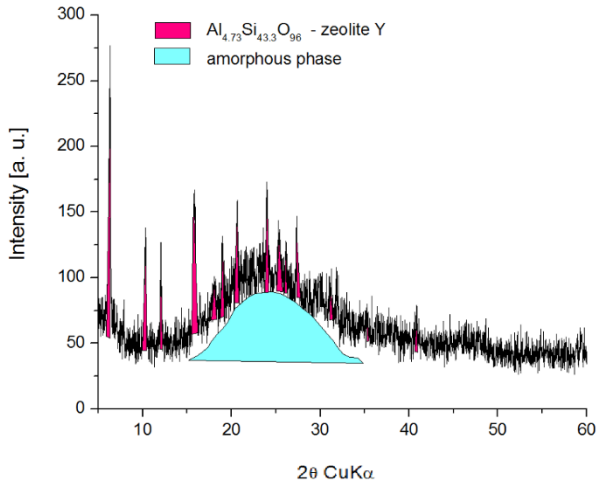

Fig. 3. Diffractogram of spent zeolite-based catalyst

The observed intensity and definition of the diffraction peaks confirm that a part of the original zeolite framework remains structurally intact. Consequently, the broad diffuse scattering (amorphous halo) in the 2ϑ range of 15–35° indicates the presence of an amorphous phase, corresponding to the structural degradation and partial collapse of the primary zeolitic network [21]. Therefore, the spent catalyst can be described as a composite material, consisting of a residual high-silica zeolitic phase embedded in an amorphized aluminosilicate matrix, which still retains a certain level of microporous organization [22].

3.2 Sintering Behaviour of Waste Zeolite Catalyst and Kaolin

To determine the sintering temperature ranges of the waste catalyst and kaolin, samples of each raw material were prepared by uniaxial pressing in a metal die at 100 MPa. The green bodies were heat treated in air at 1250, 1350, and 1400 °C with an isothermal hold of 30 min. The physicochemical properties of the investigated samples are summarized in Table 3. At 1250 °C, the catalyst samples exhibited relatively high porosity (30.92 %) and low density (1.84 g/cm³). A significant increase in densification was observed between 1250 °C and 1350 °C, with the apparent density rising to 2.23 g/cm³ and the apparent porosity decreasing to 14.98%. Further densification occurred at 1400 °C, resulting in a density of 2.33 g/cm³ and a porosity of 7.04 %.

Table 3. Physicochemical properties of the spent catalyst and kaolin at various sintering temperatures

Sample	*T*, °C	$\rho_{app.}$, g/cm³	*WA*, %	$P_{app.}$, %
catalyst	1250	1.84	16.76	30.92
	1350	2.23	6.72	14.98
	1400	2.33	3.01	7.04
kaolin	1250	1.64	23.52	38.57
	1350	1.81	17.36	31.42
	1400	1.93	13.10	25.28

*T – temperature; *WA* – water absorption; $P_{app.}$ – apparent porosity; $\rho_{app.}$– apparent density

Based on the apparent density and apparent porosity data in Table 3, the optimal sintering temperature for the spent catalyst was determined to be 1400 °C, as it provides maximum densification before the possible onset of microstructural degradation (bloating) that typically occurs at higher temperatures due to decomposition of crystalline phases and release of gaseous species. For these reasons, the pure catalyst was not subjected to firing at 1450 °C and 1500 °C.

For kaolin, the sintering behaviour followed a similar trend but with a different densification pattern. At 1250 °C, the samples exhibited an apparent density of 1.64 g/cm³ and an apparent porosity of 38.57 % (*WA* = 23.52 %). As the firing temperature increased to 1350 °C, the density rose to 1.81 g/cm³ and the porosity decreased to 31.42 % (*WA* = 17.36 %). This trend reflects the evolution of the kaolin matrix through dehydroxylation, transformation to metakaolin and spinel, and subsequent mullite formation. Overall, the kaolin samples exhibited lower density and higher porosity compared to the pure catalyst. For instance, at 1400 °C, the apparent density of kaolin was 1.93 g/cm³, significantly lower than the 2.33 g/cm³ achieved for the pure catalyst.

The spent catalyst exhibits superior sintering behavior compared to kaolin, characterized by higher apparent density and lower apparent porosity across all investigated temperature ranges (1250–1500 °C). This is attributable to the specific chemical composition and phase behavior of the two materials. The catalyst does show a gradual mass loss of about 10 % between 250 and 900 °C

(Fig. 2); this loss is due to the slow combustion of residual carbon compounds, not to the evolution of structural water. The release of structural water from kaolin creates transient porosity and internal stresses, which hinder intimate particle contact and retard sintering kinetics. In contrast, the spent catalyst, having already undergone high-temperature service, does not evolve gases during firing, allowing for the early formation of dense particle-to-particle contacts. Furthermore, the catalyst contains a significant amount of rare-earth oxides (approximately 3.43% La_2O_3 and other REOs). In the Al_2O_3-SiO_2 system, these oxides form low-melting eutectics that reduce the viscosity of the liquid phase, thereby accelerating liquid-phase sintering. Kaolin relies on traditional fluxing oxides (K_2O, CaO, Na_2O, MgO) present in a lower total amount (1.75 %).

Finally, the spent catalyst possesses a partially preserved zeolitic framework that transforms directly into mullite and corundum upon heating. In contrast, kaolin undergoes a sequence of phase transitions—from metakaolin (~600 °C) to a spinel phase (~950 °C)—before finally forming mullite (>1200 °C) [23]. Each transition in kaolin involves volume changes and structural rearrangements that induce internal stresses and potential instability. The absence of such intermediate phases in the catalyst's thermal evolution minimizes these effects, thereby accelerating densification.

3.3 Characterization of Catalyst-Kaolin Compositions

Thermal analysis of the studied compositions, C_{30}, C_{50}, and C_{70}, carried out up to 1250 °C in an air environment at a heating rate of 10 °C/min (Fig. 4–6), revealed pronounced changes in thermal behavior due to the changing ratio between kaolin and spent zeolite catalyst. Analysis of TG–DSC thermograms shows that thermal processes take place in several characteristic temperature ranges, typical of aluminosilicate systems with varying content of structural and residual volatile components. In the low-temperature range (100–200 °C), all compositions exhibit a minor mass loss associated with the release of physically adsorbed moisture. At approximately 500 °C, a distinct endothermic effect was recorded, accompanied by significant mass loss, which is associated with the dehydroxylation of kaolinite [24].

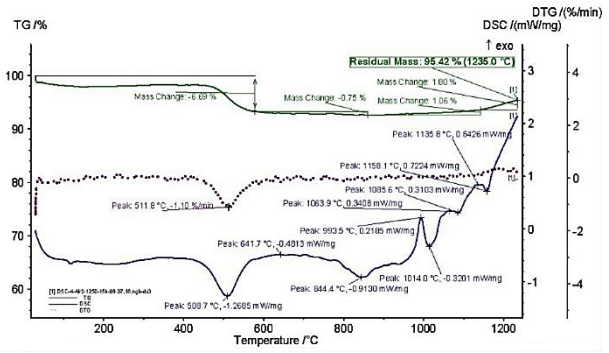

Fig. 4. TG-DSC curves of sample C_{30} up to 1250 °C

Quantitative analysis of the TG curves shows that this process is most pronounced in composition C_{30} (Fig. 4), where the mass loss reaches 6.69 %, accompanied by an intense endothermic DSC peak at 508.7 °C. As the content of the waste zeolite catalyst increases, the intensity of this effect decreases. At C_{50} (Fig. 5), the mass loss is 4.35 %, and for C70 (Fig. 6), the process is only weakly pronounced, with a loss of only 2.39 %. This trend directly correlates with the decreasing kaolin content and the increasing dominance of the thermally more stable catalyst matrix. The observed temperature ranges and mass losses are in good agreement with the published data on kaolinite dehydroxylation (495–550 °C, 12.8–13.0 %) [23].

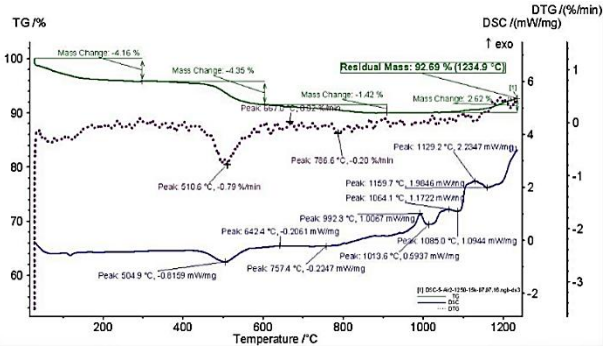

Fig. 5. TG-DSC curves of sample C_{50} up to 1250 °C

In the high-temperature region (1000–1100 °C), compositions C_{30} and C_{50} show pronounced exothermic effects associated with the formation and growth of the mullite phase ($3Al_2O_3 \cdot 2SiO_2$) [25]. The most intense peak was recorded at 993.5 °C for C_{30} and at 992.3 °C for C_{50}, which is fully consistent with the literature data on mullite nucleation. Similar results have been reported by other authors, who identified an exothermic peak of about 988 °C [26], interpreted as the onset of mullite crystallization.

In contrast, for composition C_{70}, the exothermic effects associated with mullite formation are strongly suppressed (Fig. 6). This is probably

attributed to the inhibiting action of La_2O_3 on mullite nucleation.

The presence of La_2O_3 (1.18 %) is known to increase the crystallization temperature of the amorphous aluminosilicate matrix and inhibit nucleation of mullite, thereby stabilizing the amorphous structure [27].

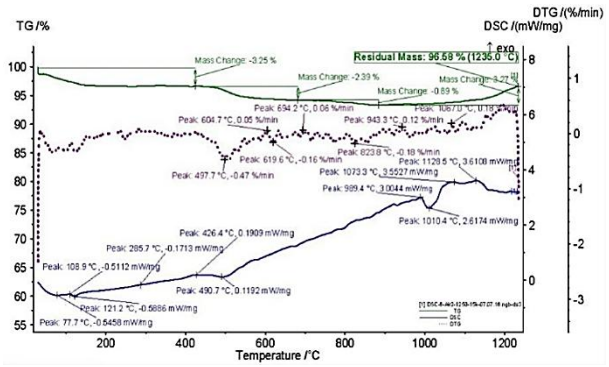

Fig. 6. TG-DSC curves of sample C_{70} up to 1250°C

The lower content of Fe_2O_3 (0.64 %) does not promote crystallization at these temperatures, as it likely remains dissolved in the amorphous phase or is incorporated into the mullite solid solution without acting as a nucleation agent [28, 29]. Consequently, the combined effect of these oxides, particularly the dominant stabilizing role of La_2O_3, suppresses the exothermic mullite formation peak, resulting in a predominantly amorphous structure up to 1250 °C.

The influence of the spent catalyst on the phase composition after firing at 1350 °C is illustrated by the XRD patterns in Figs. 7–9. All three compositions contain mullite ($3Al_2O_3{\cdot}2SiO_2$), cristobalite (SiO_2), and residual quartz (SiO_2) as the primary crystalline phases.

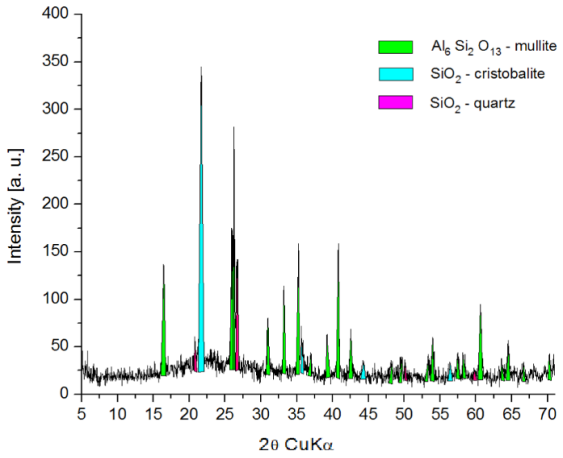

Fig. 7. XRD pattern of sample C_{30} at 1350 °C

For sample C_{30}, the diffraction pattern is dominated by strong quartz reflections, accompanied by moderate mullite and cristobalite peaks.

An increase in the catalyst content (sample C_{50}) leads to a pronounced modification of the phase composition: the quartz content decreases, while the amount of cristobalite increases significantly. Although the intense reflection at ~26.6° 2ϑ probably contains overlapping contributions from both residual quartz and cristobalite, this change is confirmed by the decreasing intensity of the small quartz peaks (around 20.8° and 25.3° 2ϑ) and the simultaneous increase of the primary cristobalite peak intensity at ~22.0° 2ϑ. Notably, this composition exhibits the highest mullite content. The main reason for this behavior is the optimal 1:1 ratio of kaolin to spent catalyst in C_{50}. The reactive alumina and fluxing oxides from the kaolin interact with the catalyst's partially amorphous structure to create a low-viscosity liquid phase. This liquid phase promotes the dissolution of quartz and accelerates mullite crystallization [28, 30]. The well-defined mullite reflections observed for C_{50} (Fig. 8) are in good agreement with the pronounced exothermic peak detected in the DSC curve (Fig. 5).

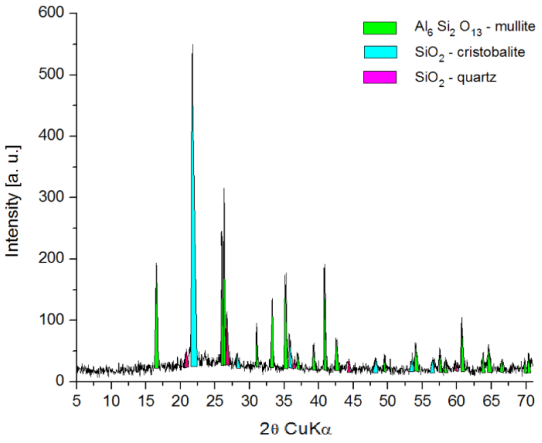

Fig. 8. XRD pattern of sample C_{50} at 1350 °C

With a further increase in catalyst content (sample C_{70}), the phase composition differs significantly. As shown in Fig. 9, quartz reflections are absent, cristobalite becomes the dominant phase, and the mullite peaks are less intense than in C_{50}. Although C_{70} has the highest total Al_2O_3 content (36.33 mass%, Table 1), the mullite yield does not increase. This is attributed to the lower kaolin fraction (30 mass%), which is the primary source of the reactive amorphous alumina formed during dehydroxylation [31] and is essential for extensive mullite crystallization. In contrast, the Al_2O_3 present in the spent catalyst is less reactive, as it remains part of a thermally stable aluminosilicate matrix [14].

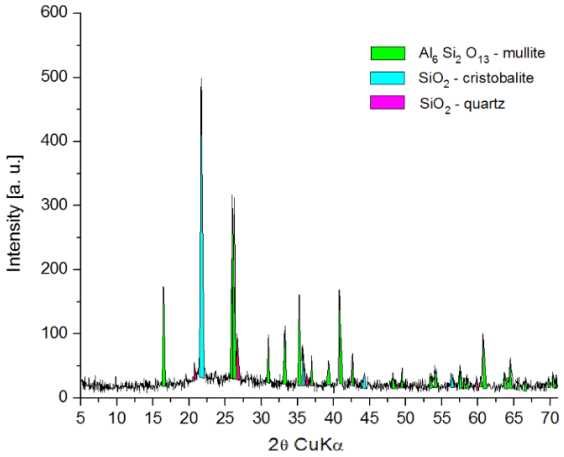

Fig. 9. XRD pattern of sample C_{70} at 1350 °C

The physicochemical properties of the synthesized materials are strongly influenced by the specific catalyst-kaolin ratio and the firing temperature. For all studied compositions, increasing the temperature leads to a consistent trend of higher apparent density, accompanied by a reduction in both apparent porosity and water absorption (Table 4). Sample C_{30} had the highest apparent density at 1250°C, with a value of 2.26 g/cm³. Compositions C_{50} and C_{70} had values of 2.25 g/cm³ and 2.17 g/cm³, respectively. The most pronounced density increase occurs in the 1350–1500 °C range—from 2.26 to 2.38 g/cm³ for C_{30}, from 2.25 to 2.31 g/cm³ (C_{50}), and from 2.17 to 2.29 g/cm³ (C_{70}). The observed increase in density is directly related to the increase in firing temperature. Higher temperatures accelerate diffusion processes, leading to pore closure and coalescence of micropores, i.e., to densification of the material.

Table 4. Physicochemical properties of samples C_{30}, C_{50}, and C_{70} at various sintering temperatures

T, °C	Sample	$\rho_{app.}$ (g/cm³)	*WA*, %	$P_{app.}$, %
1250	C_{30}	2.26	5.35	12.09
	C_{50}	2.25	5.92	13.32
	C_{70}	2.17	7.38	16.01
1350	C_{30}	2.29	4.70	10.81
	C_{50}	2.26	5.41	12.28
	C_{70}	2.25	5.94	13.42
1450	C_{30}	2.36	3.05	7.60
	C_{50}	2.29	3.21	6.98
	C_{70}	2.27	3.43	8.42
1500	C_{30}	2.38	2.26	5.40
	C_{50}	2.31	2.50	5.82
	C_{70}	2.29	2.61	6.03

According to the results, compositions with higher catalyst content (C_{70}) exhibit the highest initial porosity and water absorption but also show the greatest relative sensitivity to temperature-induced densification.

At the highest firing temperature (1500 °C), the differences in the apparent density between compositions become much smaller. This indicates that a comparable degree of sintering is achieved regardless of the initial composition within the studied range. The higher firing temperature leads to more effective densification, as seen from C_{30} which reached the highest apparent density of 2.38 g/cm³, the lowest porosity of 5.4 %, and the lowest water absorption of 2.26% at 1500 °C. The most significant decrease in porosity is observed in the temperature range of 1350 °C and 1450 °C, which is associated with the transition to intensive pore closure and coalescence. Composition C_{70} shows the highest initial porosity but also the largest relative decrease with increasing temperature, which confirms accelerated structural densification in this range.

Although the FCC catalyst contains fluxing oxides that promote sintering, higher catalyst additions (C_{50} and C_{70}) lead to an excessive amount of a low-viscosity liquid phase at elevated temperatures. This causes overfiring and microstructural degradation (bloating) due to gas entrapment, which increases closed porosity. The lower content of volatile or gas-evolving components in C_{30} favours a higher degree of compaction throughout the entire temperature range, which explains why C_{30} achieves the best densification performance.

The textural characteristics of the C_{30} composition were examined by nitrogen adsorption at 77 K on the raw powder mixture and on samples fired at 1250 °C and 1350 °C. The adsorption isotherms are presented in Figs. 10 and 11, and the derived textural parameters are summarized in Table 5.

Table 5. Textural parameters of the C_{30} composition

Parameter	Raw mixture	Fired at 1250 °C	Fired at 1350 °C
S_{BET}, m²/g	58.90	1.32	1.16
V_p, cm³/g	0.20	0.17	0.12

The isotherm of the raw C_{30} mixture (Fig. 10) corresponds to type II according to the IUPAC classification [21], which is characteristic of nonporous or macroporous solids.

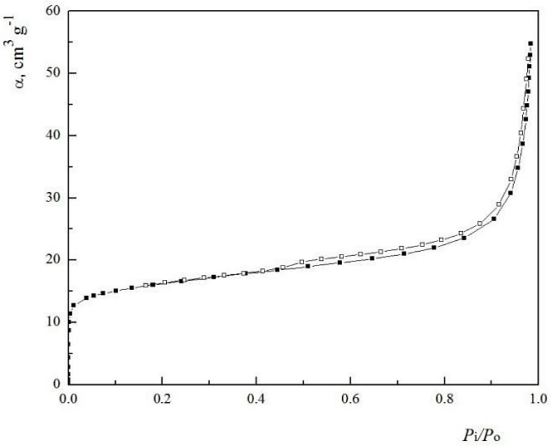

Fig. 10. Adsorption isotherm of the raw mixture C_{30}

The steep rise observed at high relative pressures indicates capillary condensation within the interparticle voids, a consequence of the fine particle size distribution and the arrangement of the particulate components. The specific surface area of the raw mixture is 58.90 m²/g, reflecting the high surface area of the spent catalyst (87 m²/g) and the inherent fineness of the kaolin.

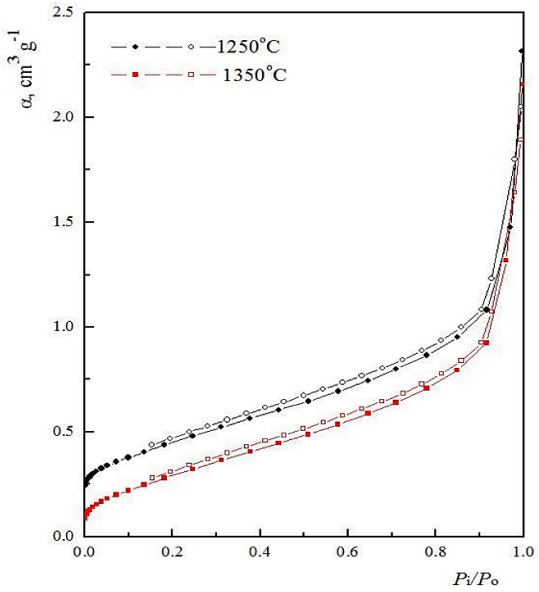

Fig. 11. Comparative adsorption isotherms of the C_{30} samples after firing at 1250 °C and 1350 °C

After firing at 1250 °C, the isotherm (Fig. 11) remains type II, but the total adsorbed volume is substantially reduced. The specific surface area decreases to 1.32 m²/g, and the total pore volume is reduced from 0.20 cm³/g to 0.17 cm³/g. Subsequent firing at 1350 °C (Fig. 11) results in only minor further changes (S_{BET}=1.16 m²/g, V_p=0.12 cm³/g).

These reductions indicate that extensive sintering occurs between 1250 °C and 1350 °C, eliminating most open porosity and forming a dense ceramic structure with only closed or very fine residual pores [22]. The textural data confirm the conclusions drawn from the physical property measurements and the phase analysis, providing direct evidence of the microstructural consolidation that occurs during liquid phase sintering.

Fig. 12 presents the dependence of flexural strength on firing temperature. A clear trend of increasing mechanical strength with temperature is observed.

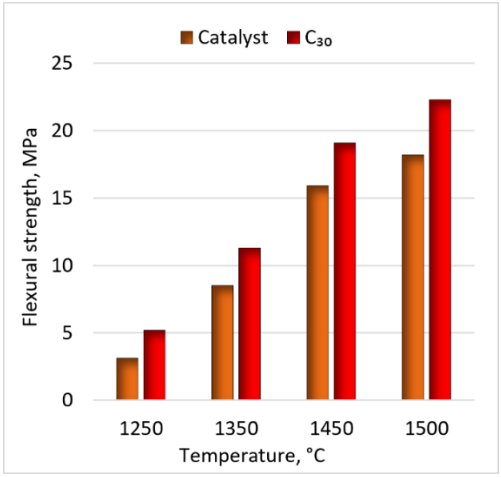

Fig. 12. Dependence of bending strength on temperature for Catalyst and sample C_{30}

The data show that sample C_{30} has higher strength values in the entire temperature range compared to the pure catalyst, which correlates with its higher density and lower porosity. This improvement is related to the optimal interaction between the kaolin matrix and the spent catalyst, which leads to the formation of a dense mullite-cristobalite structure.

4. CONCLUSION

The present investigation reveals that spent FCC catalysts modify the phase evolution and densification kinetics of kaolin-based ceramic systems significantly. Interaction between the aluminosilicate constituents of the catalyst with the kaolin matrix favours the crystallization of a secondary mullite-cristobalite framework. The structural transformation is driven by the formation of a transient silicate melt, which induces intensive liquid- sintering and leads to a highly consolidated microstructure with low residual open porosity.

The experimental data indicate that the final physicochemical characteristics are a direct

function of the catalyst-to-kaolin ratio. While compositions with higher catalyst content exhibit increased sensitivity to thermal treatment, the C_{30} composition demonstrates optimal densification and superior physical properties across the investigated temperature range. These findings demonstrate that spent FCC catalyst can be effectively utilized as a primary raw material for the synthesis of dense ceramic matrices. The study provides a scientific basis for the large-scale valorization of petrochemical waste, contributing to the development of resource-efficient and sustainable ceramic production processes.

CONFLICT OF INTEREST

The authors declare no conflict of interest.

REFERENCES

[1] M.S. Akhtar, S. Ali, W. Zaman, Recent Advancements in Catalysts for Petroleum Refining. *Catalysts*, 14(12), 2024: 841. https://doi.org/10.3390/catal14120841

[2] E.T.C. Vogt, B.M. Weckhuysen, Fluid catalytic cracking: recent developments on the grand old lady of zeolite catalysis. *Chemical Society Reviews*, 44(20), 2015: 7342–7370. https://doi.org/10.1039/c5cs00376h

[3] E. Aghaei, R. Karimzadeh, H.R. Godini, A. Gurlo, O. Gorke, Improving the physicochemical properties of Y zeolite for catalytic cracking of heavy oil via sequential steam-alkali-acid treatments. *Microporous and Mesoporous Materials*, 294, 2020: 109854. https://doi.org/10.1016/j.micromeso.2019.109854

[4] A. Gil, I. Sancho-Sanz, S.A. Korili, Progress and Perspectives in the Catalytic Hydrotreatment of Bio-Oils: Effect of the Nature of the Metal Catalyst. *Industrial & Engineering Chemistry Research*, 63(27), 2024: 11759–11775. https://doi.org/10.1021/acs.iecr.4c00747

[5] L. Wang, J. Guo, C. Li, R. Xiong, X. Chen, X. Zhang, Advancements and future prospects in in-situ catalytic technology for heavy oil reservoirs in China: A review. *Fuel*, *374*, 2024: 132376. https://doi.org/10.1016/j.fuel.2024.132376

[6] T. Gameiro, C. Costa, J. Labrincha, R.M. Novais, Reusing spent fluid catalytic cracking catalyst as an adsorbent in wastewater treatment applications. *Materials Today Sustainability*, 24, 2023: 100555. https://doi.org/10.1016/j.mtsust.2023.100555

[7] H. Al-Dhamri, K. Melghit, Use of alumina spent catalyst and RFCC wastes from petroleum refinery to substitute bauxite in the preparation of Portland clinker. *Journal of Hazardous Materials*, 179(1–3), 2010: 852–859. https://doi.org/10.1016/j.jhazmat.2010.03.083

[8] A. Pathak, M.S. Rana, M. Marafi, R. Kothari, P. Gupta, V. Tyagi, Waste petroleum fluid catalytic cracking catalysts as a raw material for synthesizing valuable zeolites: A critical overview on potential, applications, and challenges. *Sustainable Materials and Technologies*, 38, 2023: e00733. https://doi.org/10.1016/j.susmat.2023.e00733

[9] C. Ren, R.K. Enneti, Latest Developments in Manufacturing and Recycling of Refractory Materials. *JOM*, 73, 2021: 3401–3402. https://doi.org/10.1007/s11837-021-04890-w

[10] C. Bories, L. Aouba, E. Vedrenne, G. Vilarem, Fired clay bricks using agricultural biomass wastes: Study and characterization. *Construction and Building Materials*, 91, 2015: 158–163. https://doi.org/10.1016/j.conbuildmat.2015.05.006

[11] G. Han, S. Yang, W. Peng, Y. Huang, H. Wu, W. Chai, J. Liu, Enhanced recycling and utilization of mullite from coal fly ash with a flotation and metallurgy process. *Journal of Cleaner Production*, 178, 2018: 804–813. https://doi.org/10.1016/j.jclepro.2018.01.073

[12] B.C.A. Pinheiro, J.N.F. Holanda, Reuse of solid petroleum waste in the manufacture of porcelain stoneware tile. *Journal of Environmental Management*, 118, 2013: 205–210. https://doi.org/10.1016/j.jenvman.2012.12.043

[13] A.M.E. Khalil, M. Egiza, M.R. Diab, E. Ali, D. Xie, S. Zhang, Recycling industrial waste into sustainable high-temperature ceramics: A review of materials, processing, and circular economy strategies. *Results in Engineering*, 30, 2026: 109933. https://doi.org/10.1016/j.rineng.2026.109933

[14] S.M. Emami, A. Ramezani, S. Nemat, Recycling of spent FCC catalyst for the production of synthetic mullite. *Results in Engineering*, 30, 2026: 110053. https://doi.org/10.1016/j.rineng.2026.110053

[15] M. Ishaq, A. Ali, A.A. Hussain, K. Kamran, A. Ghuffar, A. Anwar, Industrial waste as clay substitute in brick manufacturing. *Construction and Building Materials*, 477, 2025: 141359. https://doi.org/10.1016/j.conbuildmat.2025.141359

[16] ISO 5017:2025. Dense shaped refractory products — Determination of bulk density, apparent porosity and true porosity. *International Organization for Standardization*, Geneva, Switzerland, 2025.

[17] ISO 5014:2025. Dense and insulating shaped refractory products — Determination of modulus of rupture at ambient temperature. *International Organization for Standardization*, Geneva, Switzerland, 2025.

[18] E. Restrepo, F. Vargas, E. López, C. Baudín, The potential of La-containing spent catalysts from fluid catalytic cracking as feedstock of mullite based refractories. *Journal of the European Ceramic Society*, 40(15), 2020: 6162–6170. https://doi.org/10.1016/j.jeurceramsoc.2020.04.051

[19] A. Ramezani, S.M. Emami, S. Nemat, Reuse of spent FCC catalyst, waste serpentine and kiln rollers waste for synthesis of cordierite and cordierite-mullite ceramics. *Journal of Hazardous Materials*, 338, 2017: 177–185. https://doi.org/10.1016/j.jhazmat.2017.05.029

[20] Z. Zhao, Z. Qiu, J. Yang, S. Lu, L. Cao, W. Zhang, Y. Xu, Recovery of rare earth elements from spent fluid catalytic cracking catalysts using leaching and solvent extraction techniques. *Hydrometallurgy*, 167, 2017: 183–188. https://doi.org/10.1016/j.hydromet.2016.11.013

[21] C. Buttersack, A. König, R. Gläser, Stability of a highly dealuminated Y-zeolite in liquid aqueous media. *Microporous and Mesoporous Materials*, 281, 2019: 148–160. https://doi.org/10.1016/j.micromeso.2019.02.014

[22] B.A. Holmberg, H. Wang, Y. Yan, High silica zeolite Y nanocrystals by dealumination and direct synthesis. *Microporous and Mesoporous Materials*, 74(1–3), 2004: 189–198. https://doi.org/10.1016/j.micromeso.2004.06.018

[23] E. Gasparini, S.C. Tarantino, P. Ghigna, M.P. Riccardi, E.I. Cedillo-González, C. Siligardi, M. Zema, Thermal dehydroxylation of kaolinite under isothermal conditions. *Applied Clay Science*, 80–81, 2013: 417–425. https://doi.org/10.1016/j.clay.2013.07.017

[24] P. Ptáček, F. Šoukal, T. Opravil, J. Havlica, J. Brandštetr, The kinetic analysis of the thermal decomposition of kaolinite by DTG technique. *Powder Technology*, 208(1), 2011: 20–25. https://doi.org/10.1016/j.powtec.2010.11.035

[25] A.K. Chakraborty, DTA study of preheated kaolinite in the mullite formation region. *Thermochimica Acta*, 398(1–2), 2003: 203–209. https://doi.org/10.1016/S0040-6031(02)00367-2

[26] F. Chargui, M. Hamidouche, H. Belhouchet, Y. Jorand, R. Doufnoune, G. Fantozzi, Mullite Fabrication From Natural Kaolin and Aluminium Slag. *Boletín de la Sociedad Española de Cerámica y Vidrio,* 57(4), 2018: 169-177. https://doi.org/10.1016/j.bsecv.2018.01.001

[27] Z. An, Y. Gao, J. Chen, Combined effect of La_2O_3 and Fe_2O_3 on the crystallization behavior and microstructure of CaO-MgO-Al_2O_3-SiO_2 glass-ceramics. *Ceramics International*, 51(15), 2025: 21008–21016. https://doi.org/10.1016/j.ceramint.2025.02.269

[28] Z. Liu, W. Lian, Y. Liu, J. Zhu, C. Xue, Z. Yang, X. Lin, Phase formation, microstructure development, and mechanical properties of kaolin-based mullite ceramics added with Fe_2O_3. *International Journal of Applied Ceramic Technology*, 18(3), 2021: 1074–1081. https://doi.org/10.1111/ijac.13720

[29] M. Omerašević, M. Krsmanović, N. Adamović, C.-A. Wang, D. Bučevac, Effect of Fe_2O_3 on Compressive Strength and Microstructure of Porous Acicular Mullite. *Ceramics*, 8(3), 2025: 111. https://doi.org/10.3390/ceramics8030111

[30] P.S. Behera, S. Bhattacharyya, Effect of different alumina sources on phase formation and densification of single-phase mullite ceramic – Reference clay alumina system. *Materials Today Communications*, 26, 2021: 101818. https://doi.org/10.1016/j.mtcomm.2020.101818

[31] A. Shvarzman, K. Kovler, G.S. Grader, G.E. Shter, The effect of dehydroxylation/amorphization degree on pozzolanic activity of kaolinite. *Cement and Concrete Research*, 33(3), 2003: 405–416. https://doi.org/10.1016/s0008-8846(02)00975-4